buildings

MDPI

Article

Simplified Procedure for Estimating Seismic Displacement Capacity of Concrete Piles in Wharves

Shufei Gao *, Zhenkun Huang and Yunfen Feng

School of Architecture and Civil Engineering, Liaocheng University, Liaocheng 252000, China; h18317220194@163.com (Z.H.); fengyunfen@lcu.edu.cn (Y.F.)
* Correspondence: gaoshufei@lcu.edu.cn

Abstract: The procedure of estimating the seismic displacement capacity of piles under each performance level in current wharf practices involves monitoring the material strains specified in the design criteria during nonlinear static pushover analysis with a complex numerical model. Thus, a simplified procedure for concrete piles is proposed by developing closed-form formulas for displacement ductility capacity and yield displacement of piles, while the displacement capacity is the product of ductility capacity and yield displacement. The ductility capacity assures that the pile material strain limits specified in the criteria are not exceeded. The basic form of the formula for ductility capacity is established by using the equivalent cantilever concept to model the pile–soil interaction. Then, large quantities of moment–curvature analyses of sections and pushover analyses of concrete piles were conducted to determine the related parameters in the formula by considering numerous influencing factors. The results show that the ductility capacity can be expressed as a function of the curvature ductility capacity of pile sections at the selected performance level and parameter ψ. Based on the outcomes of curvature and pushover analyses, a set of practical formulas are proposed to determine the curvature ductility capacity, which depends on the longitudinal or transverse reinforcement ratios and axial force level, along with ψ, which depends on the aforementioned factors as well as the unsupported length of the pile.

Keywords: pile-supported wharf; concrete piles; seismic displacement capacity; pushover analysis

check for updates

Citation: Gao, S.; Huang, Z.; Feng, Y. Simplified Procedure for Estimating Seismic Displacement Capacity of Concrete Piles in Wharves. *Buildings* **2024**, *14*, 3917. https://doi.org/10.3390/buildings14123917

Academic Editors: Humberto Varum and Rajai Zuheir Al-Rousan

Received: 22 October 2024
Revised: 20 November 2024
Accepted: 4 December 2024
Published: 7 December 2024

Copyright: © 2024 by the authors. Licensee MDPI, Basel, Switzerland. This article is an open access article distributed under the terms and conditions of the Creative Commons Attribution (CC BY) license (https://creativecommons.org/licenses/by/4.0/).

1. Introduction

Based on experiences from recent earthquakes in Japan and Haiti that have affected ports [1,2], significant damages to port and harbor facilities (e.g., pile-supported wharf) have dramatically shown that strong earthquakes can severely influence port facilities, with impacts ranging from minor damage to complete crippling of ports, rendering them unable to handle any cargo. The destruction of wharves may have immense effects on the economic activity of the affected regions and countries. Because of the growing recognition that wharves can behave poorly in major earthquakes [3], there is an emerging need to develop criteria or codes for assessing the seismic performance of wharf structures. The recent seismic design criteria or codes for wharves have used a displacement-based design method [4,5]. In this method, seismic analysis of wharf structures is performed for each seismic hazard and performance level to determine the displacement demand and capacity at the deck level, while the displacement capacity exceeds the displacement demand. The performance levels of structures are related to the strains of the pile materials in the plastic hinge zones, and the displacement capacity of piles is determined by the material strain at a given performance level. A rigorous evaluation of the capacity requires nonlinear static pushover analysis of the pile modeled with significantly small elements in order to capture accurately the plastic hinge length and the section curvature at each load step. The displacement capacity can be determined at the instant when one of the pile materials, which compose the critical section of the plastic hinge, reaches the strain limit value for

a performance level. Moreover, the complex soil–pile interaction is included in pushover analysis. Thus, the continuous monitoring of material strains during seismic analysis is very difficult for most commercial structural analysis programs [6,7] and is not appropriate for preliminary or iterative design.

In order to avoid direct monitoring of material strains during analysis, simplified procedures have been developed based on different simplifications of modeling and assumptions. Due to the sloping dike of wharves and large rigidity of wharf decks, the landside pile has the shortest unsupported length, resulting in the first formation of a plastic hinge in the landside pile. Consequently, the capacity analysis of wharves can be performed with the landside single pile rather than an entire wharf model. The existing simplified procedures are all based on the analysis of single piles. The wharf design criteria for the Port of Long Beach [4] determines the displacement capacity from the curvature of the critical section at the plastic hinge location for a performance level, the yield displacement, and an assumed plastic hinge length. The yield displacement is determined from the pile's initial position to the formation of the plastic hinge being considered during pushover analysis. It is evident that the procedure still performs pushover analysis but without monitoring material strains. Additionally, the procedure cannot be used for piles with a large unsupported length and in-ground and top hinges having a ratio $M_{\text{p, in-ground}}/M_{\text{p, top}} > 1.25$, where $M_{\text{p, in-ground}}$ and $M_{\text{p, top}}$ are the pile bending moment at the in-ground and pile top plastic hinge, respectively [4]. Furthermore, Goel [6] developed a procedure with closed-form formulas for piles with partial moment connection used in marine oil terminals. These formulas utilize the displacement ductility capacity (factor) at the selected performance level and parameters depending on the relative stiffness and strength of the pile and the connection. The procedure needs to conduct section analysis to determine the moment–rotation relationship of the partial moment connection, and the formulas are all derived based on the equivalent depth-of-fixity assumption without detailed modeling of the soil–pile interaction. Thus, the procedure seems to be a bit complicated and limited to particular applications. However, estimating displacement capacity with displacement ductility capacity offers a new way of avoiding complex pushover analysis.

Different from piles in wharves, numerous investigations on the displacement ductility capacity (factor) of piles in bridge foundations have been conducted by either experimental tests or numerical analyses. Budek et al. [8] studied the displacement ductility capacity of a reinforced pile with a diameter of 1.83 in cohesionless soil based on the elastic Winkler beam model, and the ductility capacity corresponded with the maximum allowable concrete strain predicted by the moment–curvature analysis. Their study did not incorporate the influence of the longitudinal reinforcement ratio and axial force level. Chai [9] developed a relationship between the displacement ductility of extended pile shafts and the curvature ductility of the pile section based on the equivalent cantilever concept, as well as a concentrated plastic hinge model with a prescribed hinge length. In order to validate the relationship proposed by Chai [9], Chai and Hutchinson [10] conducted an experiment to investigate the ductility capacity of reinforced concrete piles in sandy soils. Afterwards, Chai and Song [11] studied the curvature ductility capacity of extended pile shafts in cohesive soils and concluded that curvature ductility demand is not sensitive to the longitudinal reinforcement ratio or axial force level and is independent of pile diameter. Song et al. [12] also proposed a model relating the displacement ductility factor of piles to the local curvature ductility of sections, and the concentrated plastic hinge model and elastic soil springs were utilized to characterize pile nonlinearity and the soil–pile interaction, respectively. Then, Song et al. [13] studied the displacement ductility of piles in cohesionless soils for two specified performance levels based on the model by Song et al. [12] and recommended a set of design ductility limits for various levels. However, the location of the maximum moment in piles may vary due to the effects of the soil–pile interaction, and utilization of the concentrated plastic hinge method in simulating the nonlinear flexural behavior of piles gives unsatisfactory results [14]. During ductility capacity analysis with the concentrated plastic hinge model, the calculated ductility depends on the value of the plastic hinge

length. The influence of a changing plastic zone for piles cannot be incorporated in the concentrated hinge model with a constant plastic length. In order to avoid the impact of plastic hinge length, Chiou et al. [15] studied the displacement ductility capacity of piles in clay based on the distributed plastic hinge model, which placed hinges along potential plastic regions of piles. In the study, the impact of the transverse steel ratio and unsupported length of pile was not considered.

Considering that evaluating the displacement capacity of piles with the ductility capacity seems to be ingenious, this study developed a new relationship between the ductility capacity of concrete piles in wharves with the curvature ductility capacity of pile sections based on the equivalent cantilever concept for the soil–pile interaction. Then, parametric analyses were conducted to investigate the influence of pile diameter, longitudinal and transverse reinforcement ratio, axial force level, pile-unsupported length, and soil stiffness on the basis of nonlinear static pushover analyses for a fixed-head pile in homogeneous soil. The distributed plastic hinge model and inelastic lateral soil (p–y) springs are included in the modeling of piles. Detailed pushover analyses were performed to obtain pushover curves and corresponding ductility capacities under three performance levels specified in ASCE/COPRI 61-14 [5]. Finally, closed-form formulas for the parameters in the developed relationship are proposed for all performance levels.

2. Derivation of Equation for Displacement Ductility Capacity of Concrete Piles

Cast-in-drilled-hole concrete piles are widely used in wharves from China and some other countries. The longitudinal reinforcing bars of piles are extended from the piles into the wharf deck or pile cap to develop the pile-to-deck connection. Since the wharf deck is much stiffer than the piles, fixed rotations at the heads of the piles are considered in this study. For the seismic analysis of wharves under a horizontal ground motion, the soil-pile system is modeled as the beam on a nonlinear Winkler foundation, as shown in Figure 1a, in which the force–deformation relationship of the soil springs is utilized to represent the surrounding soil properties. The relationship is developed by the so-called p–y curves, which express the contact pressure p at the pile–soil interface for a given deformation y and depth. Under horizontal earthquake exciting, the lateral force F associated with the inertial response of the wharf superstructure generates a bending moment distribution that depends on the pile height above ground level (L_u) and the relative soil-pile stiffness, as illustrated in Figure 1a. The height at the maximum moment is a potential location for the plastic hinge, which is a critical parameter for the seismic design. It is evident that a plastic hinge will form first at the top of the pile for fixed head condition. Then another plastic hinge will develop in the ground at the point of the maximum moment. In order to obtain a convenient closed-form equation for displacement ductility capacity, the pile-soil system in Figure 1a can be represented by a simple model based on the concept of an equivalent cantilever, as shown in Figure 1b, in which the pile is assumed to be fixed at the bottom at a depth equal to the equivalent depth to the point of fixity (L_f) below the ground level. Thus, a plastic hinge will develop first at the top of the pile, then another one will later form at the base. In the light of the deflected shape of the pile under lateral force F, the displacement capacity Δ_c, which is the maximum lateral displacement that occurs at the top when the material strains at the top hinge do not exceed the values specified for a given performance level, can be the sum of the yield displacement Δ_y and the plastic displacement Δ_p, i.e.,

$$\Delta_c = \Delta_y + \Delta_p \quad (1)$$

The pile yield displacement Δ_y can be determined from the pile's initial position to the formation of the first plastic hinge. Considering that the curvature distribution of the pile is fixed at the base before the first hinge forms, Δ_y can be calculated by Equation (2), where α is a coefficient that accounts for the effect from the simplification of the soil-pile system with an equivalent cantilever beam, and ϕ_y is the yield curvature of pile sections.

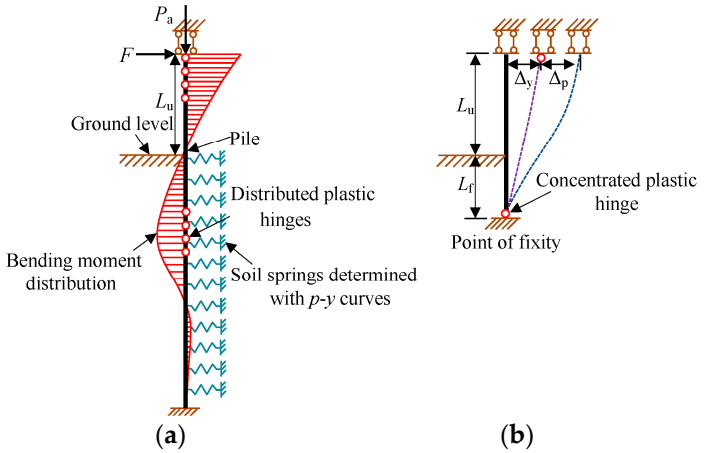


Figure 1. Beam model on nonlinear foundation and equivalent fixity model. (**a**) Beam model on nonlinear foundation. (**b**) Equivalent fixity model.

$$\Delta_y = \alpha \frac{1}{6} \phi_y (L_u + L_f)^2 \tag{2}$$

The pile plastic displacement Δ_p arises from the rotation of the plastic hinge, which is the product of the plastic curvature ϕ_p and plastic hinge length L_p. Then, Δ_p can be determined as follows:

$$\Delta_p = \phi_p L_p \beta (L_u + L_f) \tag{3}$$

where $\phi_p = \phi_m - \phi_y$, in which ϕ_m is the total curvature when the material strains reach the limits specified at the given performance level, and ϕ_y is the yield curvature; β is also a parameter that considers the influence of the equivalent representation of the soil-pile system with a simple model. There are numerous equations for calculating the plastic hinge length L_p. In the study, the equation from POLB [4] for concrete piles is adopted as follows:

$$L_p = 0.08 L_c + 0.022 f_y d_b \tag{4}$$

where L_c is the the distance from the center of the pile top plastic hinge to the point of contraflexure in the pile, f_y is the yield strength of the reinforcing bar in MPa, and d_b is the diameter of the longitudinal bar in meters.

Thus, for a given performance level, the corresponding displacement ductility capacity μ_Δ of the pile can be given by:

$$\mu_\Delta = \frac{\Delta_c}{\Delta_y} = \frac{\Delta_y + \Delta_p}{\Delta_y} = 1 + \frac{\Delta_p}{\Delta_y} \tag{5}$$

By substituting Equations (2) and (3) into Equation (5), it can be rewritten as:

$$\mu_\Delta = 1 + \frac{6\beta\phi_p L_p}{\alpha\phi_y (L_u + L_f)} = 1 + \frac{6\beta(\phi_m - \phi_y) L_p}{\alpha\phi_y (L_u + L_f)} \tag{6}$$

By simplifying the above equation with Equation (4), μ_Δ can be obtained as follows:

$$\mu_\Delta = 1 + \frac{6\beta}{\alpha}\left(\frac{\phi_m}{\phi_y} - 1\right)\frac{L_p}{(L_u + L_f)} = 1 + \frac{6\beta}{\alpha}(\mu_\Phi - 1)\frac{(0.08 L_c + 0.022 f_y d_b)}{(L_u + L_f)} \tag{7}$$

where μ_Φ is the curvature ductility capacity of pile sections. Since the piles in wharves are generally very long, the second term in Equation (4) seems to be negligibly small.

Meanwhile, it is assumed that L_c is equal to the sum of L_u and L_f. Then, Equation (7) can be further simplified as follows:

$$\mu_\Delta = 1 + \frac{0.48\beta}{\alpha}(\mu_\Phi - 1) \tag{8}$$

By defining parameter $\psi = 0.48\beta/\alpha$, μ_Δ can be finally expressed as follows:

$$\mu_\Delta = 1 + \psi(\mu_\Phi - 1) \tag{9}$$

3. Modeling and Validation of Soil-Pile System

3.1. Modeling Method

For the displacement ductility capacity of piles, the closed-form equation, i.e., Equation (9), has been developed based on the equivalent fixity model. However, several parameters (i.e., α, ψ) resulting from the development process still need to be determined. Since too many influencing factors can be incorporated in the study of the displacement capacity of piles, numerical investigation may be a more effective means than experimental tests. For the concrete piles in wharves, the displacement ductility capacity with various influencing factors is estimated through detailed pushover analysis. In this investigation, the analysis model is created based on the beam model on a nonlinear Winkler foundation, as shown in Figure 1a, in which the pile is modeled by beam elements with distributed plastic hinges to describe pile nonlinearity, and the soil resistance is modeled by a suite of independent soil springs constructed by p–y curves. The curves from API [16] are utilized to develop the force–deformation relationship of springs, as shown in Figure 2, in which P_i is the soil per unit length reaction of the i-th pile element, and $f_{i,S}$ and y_i are the force and deformation for the i-th spring, respectively. The spacing of the soil springs is determined based on the recommendation from POLB [4]. The first soil spring is located at 15 cm below the ground level, then springs are spaced at 30 cm to the depth of 3 m. Below that, the spacing is increased to 60 cm. The distributed plastic hinges utilized in the study can model the spread of plasticity in the pile during lateral loading. The plastic hinge length is assigned on the basis of the spacing of the hinges, which distributes over a region where plasticity may develop during loading. In order to consider the axial force at the pile top from the superstructure, an axial force P_a is applied at the top of the pile, as illustrated in Figure 1. Finally, modeling of the pile-soil system is accomplished by the program SAP2000.

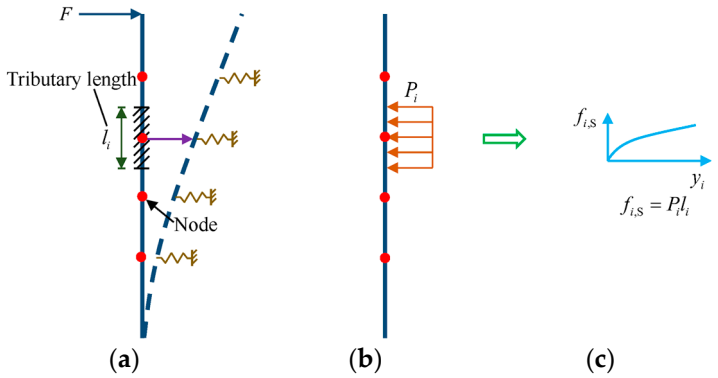


Figure 2. Determination of force–deformation relationship for soil springs. (**a**) Discretized pile. (**b**) Soil reaction distribution. (**c**) f_S–y curve.

3.2. Validation of Modeling Method

The reliability of the modeling method was verified by comparing its results with test results from the literature. The full-scale lateral loading tests for concrete piles from Tuladhar et al. [17] were adopted for validation. Detailed information about the tests is referred to in that study. The modeling method described above was used to model the test pile, and moment–curvature analysis of pile sections and pushover analysis of

piles were performed. The computational results of the numerical model constructed by the aforementioned method were compared with the experimental results, as shown in Figures 3 and 4. It can be seen that little difference can be found between the computational and experimental results. It can be concluded that the modeling method can reliably describe the soil-pile system.

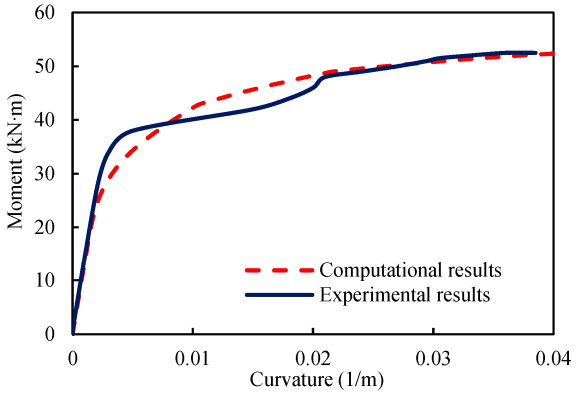


Figure 3. Comparison of moment–curvature curves.

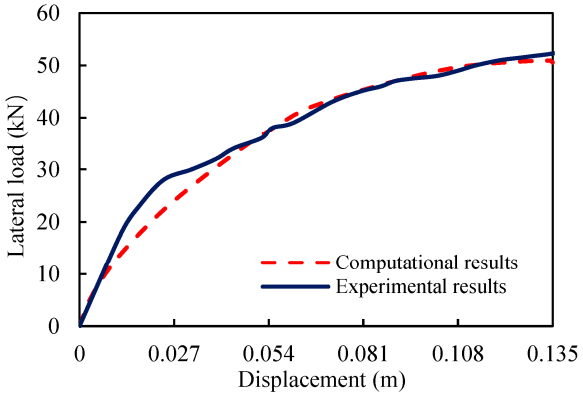


Figure 4. Comparison of pushover curves.

4. Moment–Curvature Analysis and Curvature Ductility Capacity of Pile Sections

4.1. Section Characteristics

The commonly used cast-in-drilled-hole concrete piles in China were studied for curvature ductility capacity. The main parameters of the piles are listed in Table 1. The piles are circular with a diameter of D = 0.8, 1.0, or 1.2 m and are reinforced with a longitudinal steel ratio of ρ_l = 1~3% and a transverse steel ratio of ρ_s = 0.6~2%. The longitudinal steel has a Chinese grade HRB400 with a yield strength of 400 MPa, while the transverse spiral steel possesses a grade HPB300 with a yield strength of 300 MPa. The piles are cast by concrete with a Chinese grade C40, the compressive strength of which is taken as $f_c' = 26.8$ MPa. Furthermore, the piles are loaded by an axial force P_a, which equals 10%, 20%, or 30% of its axial bearing capacity $f_c' A_g$, where A_g is the gross section area. The stress–strain curves for both confined and unconfined concrete are determined by Mander's model [18], and the strain hardening equation from the literature [19] is used to describe the stress–strain curve for reinforcing steel. Figure 5 illustrates the stress–strain curves for concrete and reinforcing steel of the section with D = 0.8 m, ρ_l = 1%, and ρ_s = 0.6%.

Table 1. Dimension and material parameters of piles.

D (m)	Concrete Cover (mm)	Young's Modulus of Steel (MPa)	ρ_l/%	ρ_s/%	L_u/D	$P_a/(f_c' A_g)$
0.8, 1.0, 1.2	75	2.0×10^5	1, 2, 3	0.6, 1.3, 2	0, 2, 4, 6	0.1, 0.2, 0.3

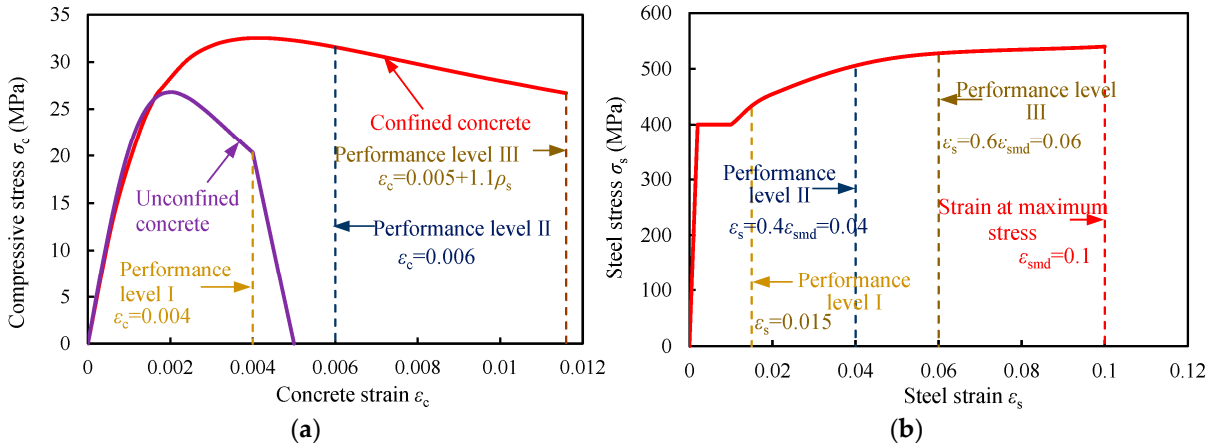


Figure 5. Stress–strain relationship for concrete and reinforcing steel bar. (**a**) Concrete. (**b**) Reinforcing steel.

4.2. Moment–Curvature Analysis

In order to ensure the seismic performance of piles, the curvature capacity of pile sections is defined as the curvature associated with the strain limit for a specified performance level. In the standard of ASCE/COPRI 61-14 [5], three performance levels are designated with different required structural responses, as described in Table 2. For the cast-in-drilled-hole concrete piles, the strain limit of each level is determined based on the recommendation of ASCE/COPRI 61-14, as listed in Table 2 and Figure 5, in which ε_{smd} is the strain at the maximum stress of the reinforcing bar and is taken as 0.1 for the bar in this study, and ε_{cu} is the ultimate concrete compression strain and is determined by the equation from ASCE/COPRI 61-14. The moment–curvature analysis can provide a curve showing the moments associated with a range of curvatures for a cross-section based on the principles of strain compatibility and equilibrium of forces. Then, moment–curvature analyses of the pile sections in Table 1 were performed to calculate the curvature capacity for each performance level. During the analyses, the moment–curvature curve was idealized by an elastic-perfectly plastic curve to determine the yield curvature ϕ_y, and the idealization was realized by the method from POLB [5], as shown in Figure 6, in which ϕ_{yi} is the curvature at the first rebar yield, M_y is the moment corresponding to ϕ_{yi}, M_p is the idealized plastic moment, and ϕ_u is the ultimate curvature of the section when $\varepsilon_c = \varepsilon_{cu}$. The yield curvature ϕ_y is determined as the curvature corresponding to the plastic moment M_p. Considering the section characteristics in Table 1, there were 81 sections for analysis. The moment–curvature curves for several sections are plotted in Figure 7, in which ϕ_I, ϕ_{II}, and ϕ_{III} are the capacities of sections at performance Level I, Level II, and Level III, respectively.

Table 2. Description of seismic performance levels of pile and material strain limits.

Performance Level	Description of Structural Response	Concrete Strain ε_c	Steel Tensile Strain ε_s
Level I	Structure exhibits near-elastic structural response with minor or no residual deformation. There is no loss of serviceability of the structure.	$\varepsilon_c \leq 0.004$	$\varepsilon_s \leq 0.015$
Level II	Structure responds in a controlled and ductile manner and experiences limited inelastic deformations at locations where repair is possible.	$\varepsilon_c \leq 0.006$	$\varepsilon_s \leq 0.4\varepsilon_{smd}$
Level III	Structure continues to support gravity loads. The damage does not prevent egress.	$\varepsilon_c \leq \varepsilon_{cu} = 0.005 + 1.1\rho_s$	$\varepsilon_s \leq 0.6\varepsilon_{smd}$

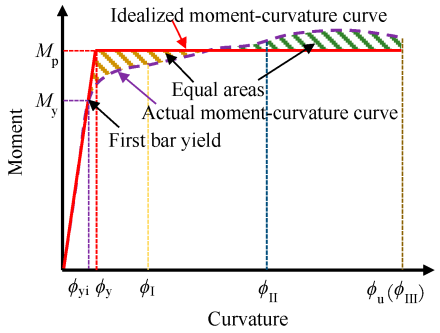


Figure 6. Idealization method for moment–curvature curve.

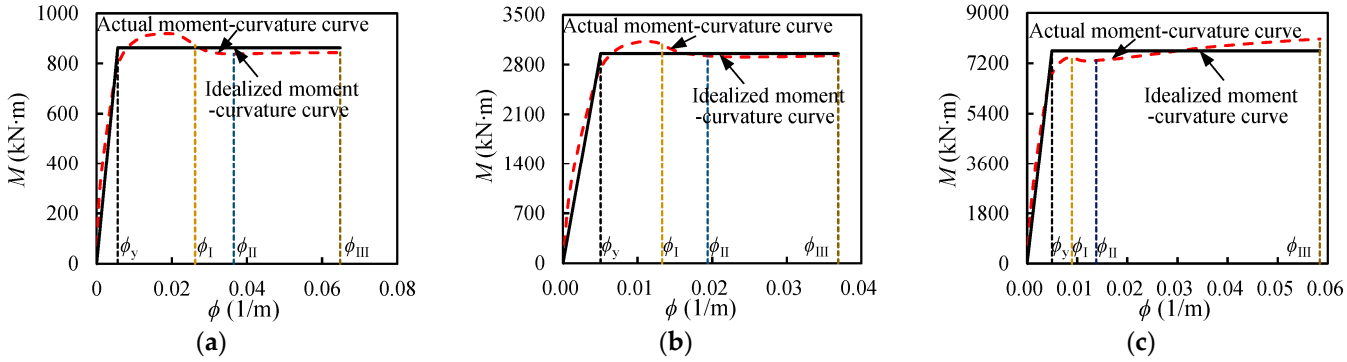


Figure 7. Moment–curvature curves for pile sections. (**a**) ρ_l = 1%, ρ_s = 0.6%, $\frac{P_a}{f_c' A_g}$ = 0.1, D = 0.8 m. (**b**) ρ_l = 2%, ρ_s = 0.6%, $\frac{P_a}{f_c' A_g}$ = 0.2, D = 1.0 m. (**c**) ρ_l = 3%, ρ_s = 2%, $\frac{P_a}{f_c' A_g}$ = 0.3, D = 1.2 m.

4.3. Curvature Ductility Capacity

Based on the results of the moment–curvature analyses, the curvature ductility capacity for each performance level could be defined as follows:

$$\mu_{\phi I} = \phi_I/\phi_y,\ \mu_{\phi II} = \phi_{II}/\phi_y,\ \mu_{\phi III} = \phi_{III}/\phi_y \tag{10}$$

where $\mu_{\phi I}$, $\mu_{\phi II}$, and $\mu_{\phi III}$ are the curvature ductility capacities of pile sections at performance Level I, Level II, and Level III, respectively.

Furthermore, a parametric study was conducted on the results of the yield curvature of pile sections. It could be found that the axial force level and reinforcing steel ratios had little impact on the yield curvature. Thus, the yield curvature could be approximately determined by Equation (11), in which ε_y is the yield strain of the longitudinal steel bar and is taken as 0.002 for HRB400 steel. The comparison between the yield curvatures from the moment–curvature analyses and those calculated by Equation (11) is presented in Figure 8. It is noted that the values from Equation (11) are quite close to those from the curvature analyses for most cases. Likewise, a parametric study was performed on the curvature ductility capacities for all three levels. It was found that the influence of pile diameter on ductility capacity was significantly minor. Thus, the ductility capacities at the three performance levels could be given by Equations (12)–(14) with the consideration of axial force level and reinforcing steel ratios. It is reminded that all variables in the equations in the paper have the units illustrated in Table 1 and the results of 27 sections with the same diameter are utilized for regression analysis.

$$\phi_y = \frac{2.629\varepsilon_y}{D} \tag{11}$$

$$\mu_{\phi I} = \frac{1}{0.064\rho_l + \frac{P_a}{f_c' A_g} + 0.055} \tag{12}$$

$$\mu_{\phi II} = \frac{1}{0.040\rho_l + 0.623\frac{P_a}{f'_c A_g} + 0.055} \quad (13)$$

$$\mu_{\phi III} = \frac{\rho_s}{0.030\rho_s - 0.111\left(\rho_l \frac{P_a}{f'_c A_g}\right)^2 + 0.197\left(\rho_l \frac{P_a}{f'_c A_g}\right) + 0.013} \quad (14)$$

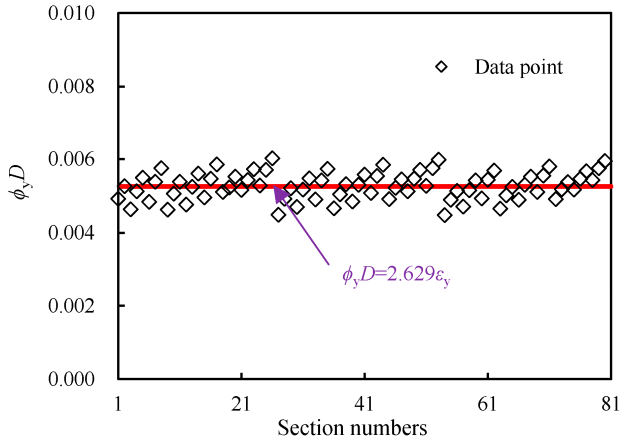


Figure 8. Yield curvatures of pile sections.

Finally, the ductility capacities estimated by Equations (12)–(14) were compared with those from the moment–curvature analyses in Figure 9, in which R^2 is the coefficient of determination with a value of around one. It was indicated that the formulas developed in the study provide an accurate evaluation of the curvature ductility capacities at all three levels. For Level I and Level II, the effect of transverse steel was too small to consider in the formulas. Then, the results with the same transverse steel ratio were averaged for analysis, resulting in the appearance of 9 data points in Figure 9a,b.

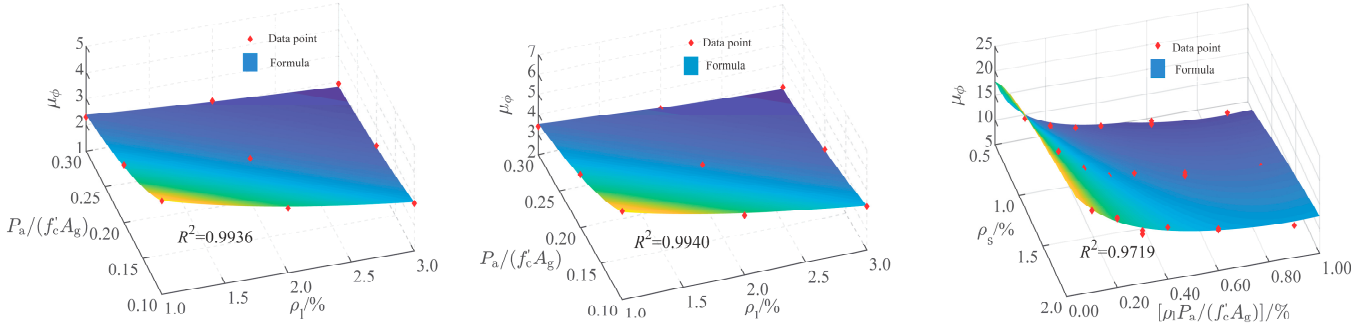


Figure 9. Curvature ductility capacities of pile sections. (**a**) Performance Level I. (**b**) Performance Level II. (**c**) Performance Level III.

5. Pushover Analyses and Displacement Ductility Capacities of Piles

5.1. Pushover Analyses

Based on the section characteristics in Table 1 and modeling method in Section 3.1, pushover analyses were performed to develop pushover curves (load–displacement curves) at the top of the pile. In order to account for the influence of the above ground height of the pile, heights of L_u = 0*D*, 2*D*, 4*D*, or 6*D* were considered in the study, as listed in Table 1. Moreover, the embedded length of the pile was taken as thirty times the pile diameter to ensure the fixity condition at the pile base, as shown in Figure 1a. To consider the impact of the soil characteristics, three types of sandy soils with various internal friction angles were included in the analyses, as given in Table 3, in which the initial modulus of the subgrade

reaction was determined by the chart from API [15]. The three soil types correspond to loose, medium dense, and dense sand, respectively. Since the majority of the wharf dike is beneath sea level, it was assumed that the all-surrounding soils of the piles were under the water table.

Table 3. Physical and mechanical parameters for sand.

Soil Types	Internal Friction Angle φ (°)	Effective Soil Weight (kN/m^3)	Initial Modulus of Subgrade Reaction (kN/m^3)
Sand-30	30	9	9400
Sand-35	35	10	20,500
Sand-40	40	11	43,500

Considering the above pile and soil conditions, there were 972 analysis cases in the study. For each case, pushover analysis was conducted to derive the pushover curve, and displacement capacity for each performance level (i.e., Δ_I for Level I, Δ_{II} for Level II, Δ_{III} for Level III) was determined by monitoring the material strain in the plastic hinge regions, as shown in Figure 10 for some cases, in which the pile section conditions are identical to those in Figure 7. The strain limits provided in Table 2 were used for the evaluation of displacement capacity in this study. During the pushover analysis, the pile yield displacement Δ_y was also calculated from the pile's initial position to the formation of the first plastic hinge being considered, as shown in Figure 10.

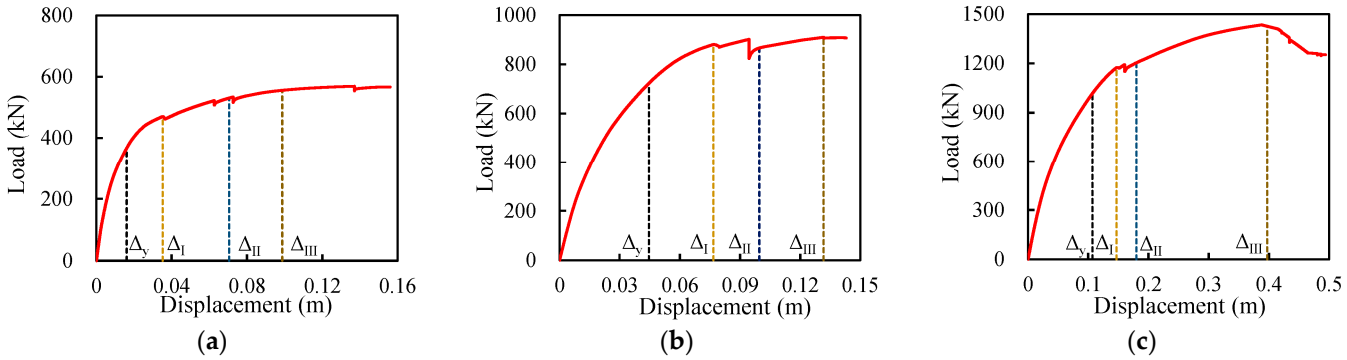


Figure 10. Pushover curves of piles. (**a**) L_u = 0D, Sand-30. (**b**) L_u = 2D, Sand-35. (**c**) L_u = 6D, Sand-40.

Furthermore, the deflected shape and bending moment distribution of the pile were determined when the displacement at the pile top reached the maximum value during analysis, as shown in Figures 11 and 12, respectively, in which the pile conditions were also identical to those in Figure 10 and ground level was taken as the elevation of zero point. It is well known that there are a lot of approaches for determining the equivalent depth to the point of fixity (L_f), which is a key parameter in Equation (2). The depth to fixity, which depends on the pile diameter and soil properties, is typically estimated from charts available in standard textbooks or from recommendations in several studies [20]. In accordance with the fixity condition at the base of the pile model in Figure 1b, the point of fixity was defined as the the location of zero-lateral deflection in the study. Then, an empirical expression for L_f was derived based on the depths for the point of fixity from the deflected shapes for all cases. It can be seen that the point of fixity with zero-lateral deflection is not at the location with the maximum moment from Figures 11 and 12.

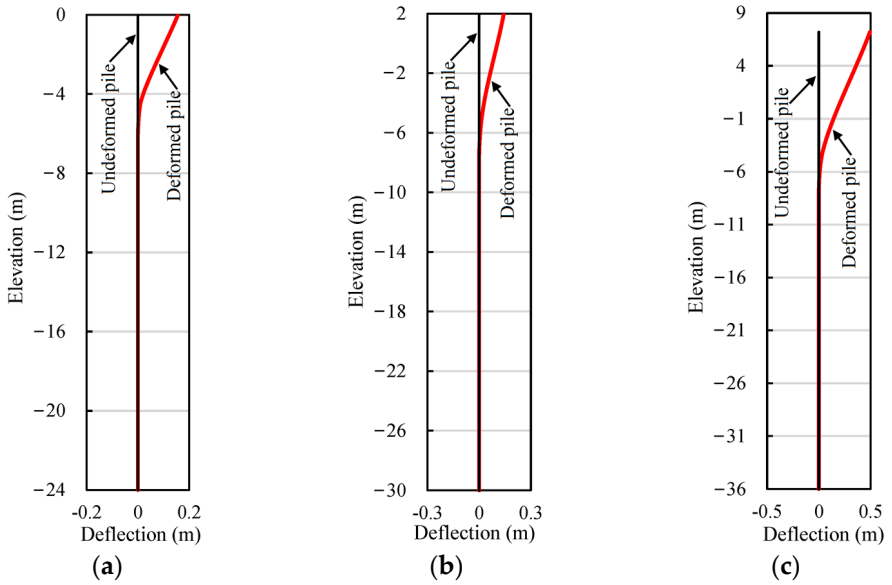


Figure 11. Deflection shapes of piles. (**a**) Sand-30. (**b**) Sand-35. (**c**) Sand-40.

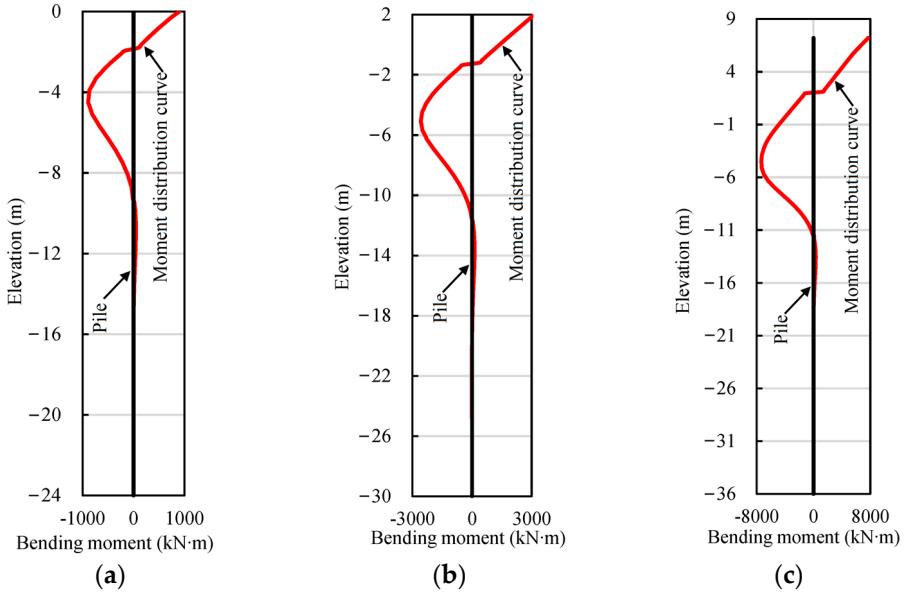


Figure 12. Bending moment distribution along pile length. (**a**) Sand-30. (**b**) Sand-35. (**c**) Sand-40.

5.2. Pile Yield Displacement

It should be noted that the pile yield displacement is expressed by the previous Equation (2), in which α and L_f are undetermined parameters. Based on the results of the depth to point of fixity from pushover analyses, it was found that the transverse steel ratio and axial load level had little impact, while the longitudinal steel ratio, pile diameter, unsupported length, and soil conditions had significant effects. Thus, L_f for the piles in this study could be estimated from Equation (15). It is reminded that all variables in Equation (15) and subsequent equations have identical units with those in Tables 1 and 3. The computational values (L_f/D) from pushover analyses and values determined by Equation (15) are compared in Figure 13, in which the data points are from the results of piles (D = 0.8 m) with the same transverse steel ratio and axial load level. It can be seen that relative error is less than 5% for most cases.

$$\frac{L_f}{D} = 0.62\rho_l - 0.25\frac{L_u}{D} - 0.12\varphi + 10.74 \quad (15)$$

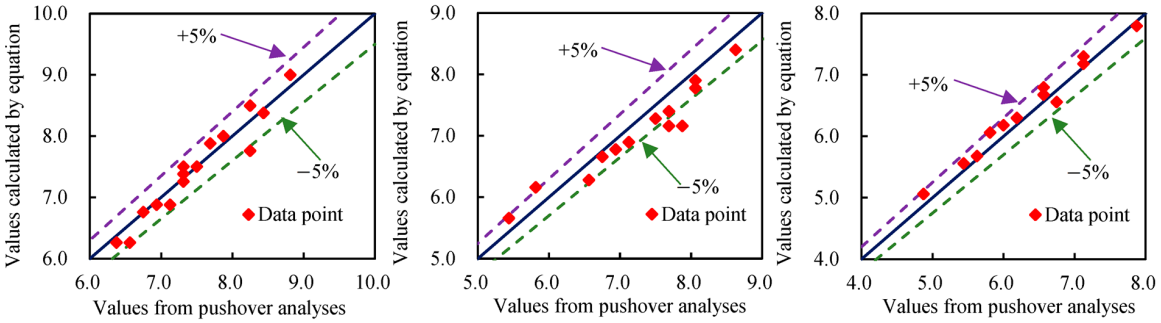


Figure 13. Depth to equivalent fixity point of pile. (**a**) Sand-30. (**b**) Sand-35. (**c**) Sand-40.

Once the yield curvature (ϕ_y) and depth to point of fixity (L_f) were separately determined by Equations (11) and (15), the dimensionless parameter α in Equation (2) could be inversely calculated by the results of the pile yield displacement Δ_y from pushover analyses. Based on the computational results of α, it was found that the soil conditions and transverse steel ratio had minor impacts, resulting in Equation (16) for α. The variable D' in Equation (16) is defined as $D' = D/1\text{m}$ to ensure the dimensional homogeneity of this formula. Finally, the pile yield displacement Δ_y could be evaluated from Equations (2), (11), (15) and (16). Based on those equations, the pile yield displacements for some analysis cases were calculated for comparison with the displacements determined by pushover analyses, as illustrated in Figure 14. It can be seen that the differences between the results from the equations and pushover analyses are minute.

$$\alpha = 0.032D'^{-1.664}\rho_l + 0.863D'^{-2.322}\left(\frac{P_a}{f'_c A_g}\right) + 0.022D'^{-1.701}\left(\frac{L_u}{D}\right) + 0.238D'^{-2.804} \quad (16)$$

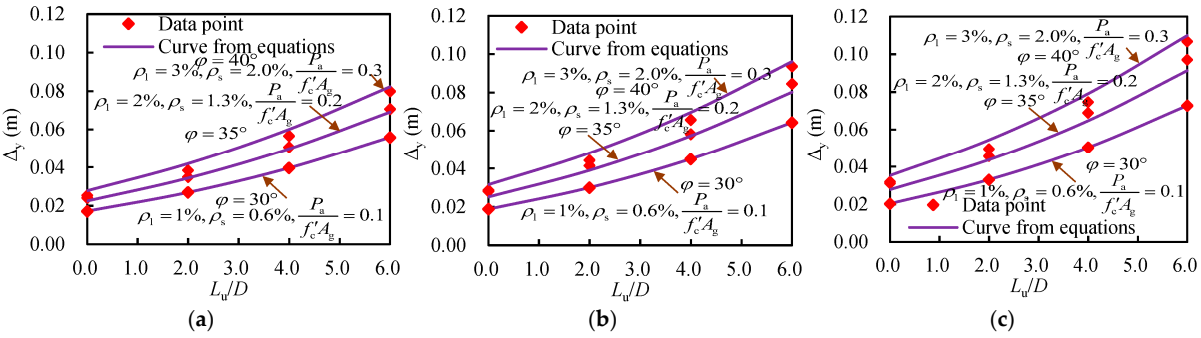


Figure 14. Yield displacements of piles. (**a**) D = 0.8 m. (**b**) D = 1.0 m. (**c**) D = 1.2 m.

5.3. Displacement Ductility Capacity

The displacement ductility capacity of the piles for each performance level can be given by:

$$\mu_{\Delta I} = \Delta_I/\Delta_y,\ \mu_{\Delta II} = \Delta_{II}/\Delta_y,\ \mu_{\Delta III} = \Delta_{III}/\Delta_y \quad (17)$$

in which $\mu_{\Delta I}$, $\mu_{\Delta II}$, and $\mu_{\Delta III}$ are the displacement ductility capacities corresponding to Level I, Level II, and Level III, respectively. Then, the ductility capacity for each performance level of each case can be obtained based on the results of the displacement capacities and yield displacements from pushover analyses. In the light of the results for the ductility capacity, the undetermined parameter ψ in Equation (9) can be back-calculated using Equations (9) and (12)–(14). For Level I, Level 2, and Level III, the parameter can be separately denoted as ψ_I, ψ_{II}, and ψ_{III}, respectively. The effect of each influencing factor

(i.e., pile diameter, longitudinal and transverse steel ratios, axial load level, unsupported length of pile, and soil condition) on parameter ψ is not discussed in detail with charts due to the limited space of the paper and tremendous analysis cases. The numerical expressions for ψ will be directly given in the subsequent sections. For Level I, it was found that the longitudinal steel ratio, axial load level, and unsupported length of the pile had significant impacts. The expression for ψ_{I} of Level I can be given by Equation (18). Based on Equations (9), (12) and (18), the displacement ductility capacities for Level I were calculated for some cases, and the corresponding results are compared with those from pushover analyses, as shown in Figure 15. The presented results in Figure 15 indicate that the above closed-form equations developed in this study can provide an accurate estimation of displacement ductility capacity. The curves for the displacement ductility capacity obtained from the closed-form equations approached the data points from pushover analyses.

$$\psi_{\mathrm{I}} = 0.062\rho_{\mathrm{l}} - 9.134\left(\frac{P_{\mathrm{a}}}{f'_{\mathrm{c}}A_{\mathrm{g}}}\right)^2 + 3.184\left(\frac{P_{\mathrm{a}}}{f'_{\mathrm{c}}A_{\mathrm{g}}}\right) + \frac{1}{0.030(L_{\mathrm{u}}/D)^3 + 10.450} \tag{18}$$

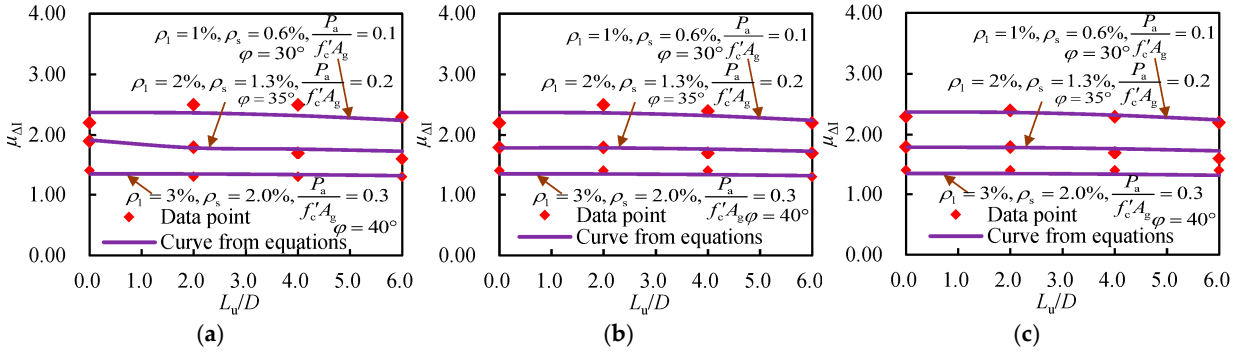


Figure 15. Displacement ductility capacity for performance Level I. (**a**) D = 0.8 m. (**b**) D = 1.0 m. (**c**) D = 1.2 m.

For Level II, the parameter ψ_{II} can also be determined with the methodology for ψ_{I}, and the expression for ψ_{II} can be given by Equation (19), in which a_1~a_7 are parameters and can be determined by Equation (20). The parameters b_i, c_i, and d_i (i = 1~7) in Equation (20) can be estimated by Table 4 or Equation (21). Since the fitting error would largely increase when all parameters were used for fitting analysis, only parameters with number i = 1~6 were fitted by formulas. Similarly, the displacement ductility capacities for Level II can be calculated by Equations (9), (12) and (19) for some cases, resulting in the curves plotted in Figure 16. The ductility capacities for those cases determined by pushover analyses are also presented in Figure 16 for comparison. It can be seen that the curves provided by the developed formulas were very close to the data points obtained from pushover analyses. Thus, it was indicated that the above developed equations for Level II can provide a good estimation of the displacement ductility capacity of concrete piles.

$$\psi_{\mathrm{II}} = a_1\rho_{\mathrm{l}}^2 + a_2\rho_{\mathrm{l}}\rho_{\mathrm{s}} + a_3\rho_{\mathrm{l}} + a_4\rho_{\mathrm{s}} + a_5\sqrt{\frac{L_{\mathrm{u}}}{D}} + a_6\left(\frac{L_{\mathrm{u}}}{D}\right) + a_7 \tag{19}$$

$$a_i = b_i\sqrt{\frac{P_{\mathrm{a}}}{f'_{\mathrm{c}}A_{\mathrm{g}}}} + c_i\left(\frac{P_{\mathrm{a}}}{f'_{\mathrm{c}}A_{\mathrm{g}}}\right) + d_i \tag{20}$$

$$\begin{cases} b_i = 29.691\sin(2.331i - 1.709) + 14.281\sin(0.693i + 3.008) \quad (i = 1, \cdots, 6);\ b_7 = 35.660 \\ c_i = 32.971\sin(2.325i + 1.428) + 16.081\sin(0.706i - 0.166) \quad (i = 1, \cdots, 6);\ c_7 = -42.710 \\ d_i = 6.362\sin(2.342i + 1.434) + 3.023\sin(0.674i - 0.099) \quad (i = 1, \cdots, 6);\ d_7 = -6.465 \end{cases} \tag{21}$$

Table 4. Values for parameter b_i, c_i, and d_i.

Parameters	i = 1	i = 2	i = 3	i = 4	i = 5	i = 6	i = 7
b_i	9.7460	−8.006	−38.260	21.950	−12.140	2.5790	35.660
c_i	−10.685	8.537	43.040	−24.310	11.950	−2.2280	−42.710
d_i	−2.1245	1.817	8.070	−4.678	3.070	−0.7617	−6.465

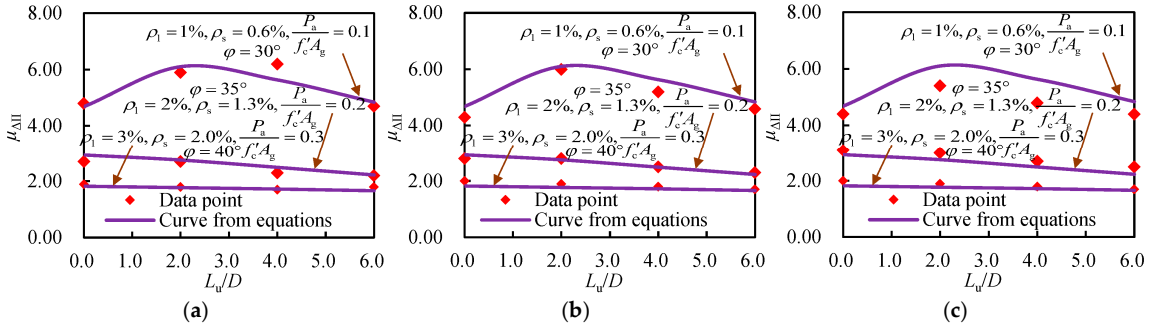


Figure 16. Displacement ductility capacity for performance Level II. (**a**) D = 0.8 m. (**b**) D = 1.0 m. (**c**) D = 1.2 m.

Following the above methodology for Level I and Level II, an expression presented in Equation (22) was developed for the parameter ψ_{III} for Level III. The parameters m_1~m_7 from Equation (22) can be computed by Equation (23), in which n_j, k_j, and q_j (j = 1~8) are parameters and can be determined by Table 5. The values in Table 5 were not fitted by a formula due to large fitting errors. The ductility capacity $\mu_{\Delta III}$ for Level III of some cases can be calculated by Equations (9), (12) and (22), resulting in the curves presented in Figure 17. The ductility capacities from pushover analyses are also provided in Figure 17 with the plotted points. The presented results in Figure 17 indicated that the formulas developed for Level III can provide a relatively accurate evaluation of the ductility capacity.

$$\psi_{III} = m_1\rho_l^2 + m_2\rho_s^2 + m_3\rho_l\rho_s + m_4\rho_l + m_5\rho_s + m_6(L_u/D)^2 + m_7(L_u/D) + m_8 \quad (22)$$

$$m_j = n_j\left(\frac{P_a}{f'_c A_g}\right)^2 + k_j\left(\frac{P_a}{f'_c A_g}\right) + q_j \quad (23)$$

Table 5. Values for parameter n_j, k_j, and q_j.

Parameters	j = 1	j = 2	j = 3	j = 4	j = 5	j = 6	j = 7	j = 8
n_j	−0.250	−6.150	10.350	−13.200	−12.400	−0.600	5.800	19.530
k_j	−0.015	2.275	−4.875	6.860	7.320	0.290	−2.750	−11.112
q_j	0.002	−0.121	0.496	−0.689	−1.053	−0.038	0.310	1.768

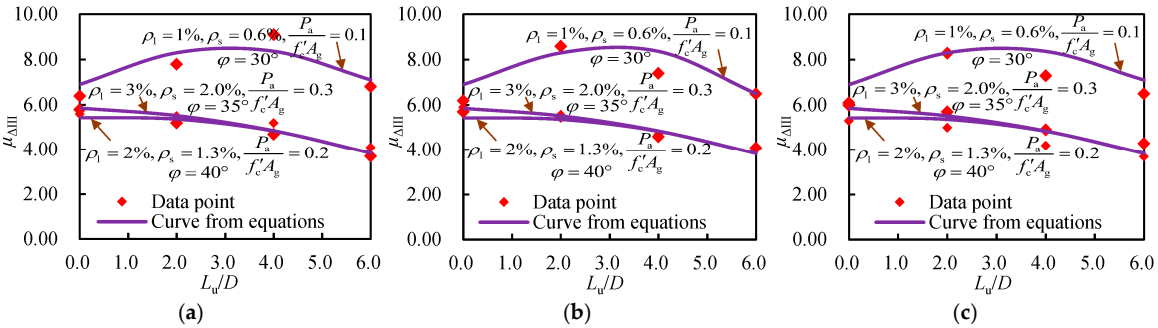


Figure 17. Displacement ductility capacity for performance Level III. (**a**) D = 0.8 m. (**b**) D = 1.0 m. (**c**) D = 1.2 m.

6. Discussion

From the figures in Section 5.2, it can be found that the transverse reinforcement ratio has no effect on the displacement ductility capacity for performance Level I but has a significant impact on the ductility capacity of Level II and Level III. This situation can be attributed to the concrete strain limits for various performance levels. The strain limits for Level II and Level III are dependent on the transverse reinforcement ratio. It is evidently that the displacement ductility capacity increases with increasing transverse reinforcement ratio. Thus, piles should be provided with adequate confining steel, especially at the pile–deck joint. The amount of transverse reinforcement should not be less than the value recommended by POLB [4] or ACI [21]. Moreover, a decrease in displacement ductility capacity with increasing longitudinal reinforcement ratio and axial load level can be generally observed for all levels. Thus, the volumetric ratio of longitudinal reinforcing steel should be limited to a reasonable range, which can be between 1% and 4%, as recommended by POLB [4]. Compared with other influencing factors, the ductility capacity decreases significantly with increasing axial load level. For Level I and Level II, the capacities are even less than 2.0 for piles with an axial load level of 0.3. Although the strain limits are not exceeded for these cases, a minimum value for displacement ductility capacity has been adopted for some seismic design practices. For instance, NZTA [22] requires that the displacement ductility capacity of piles in bridges shall be no less than 3.0 when inelastic deformation occurs at a depth greater than 2 m below the ground surface. Thus, it is recommended that the axial load level of concrete pile shall be no more than 0.3, especially for landward piles. In order to reduce the applied load from the superstructure of the wharf, the rail girder should not directly locate upon the landward pile. Furthermore, the developed formulas for displacement ductility capacity can also be utilized as limits of the displacement ductility for ductility-based design methods. From the figures presented in Section 5.2, it can be seen that the unsupported length of the pile has an appreciable effect on the ductility capacity for Level II and Level III. For these levels, the capacity decreases when the unsupported length increases. Thus, it is better not to design piles with excessively large lengths above ground level.

It is clear that the soil conditions will influence the pushover curve of piles, but its effect on the displacement ductility capacity is minor based on the pushover analysis results. Thus, the internal friction angle of sandy soil was not incorporated in the equations from Section 5.2. However, the depth to the point of fixity is related to the internal friction angle, as shown in Equation (15). In addition, all of the relationships in this study were developed based on the pile being embedded in homogeneous sand. In fact, the wharf dike consists of layered soils, while there are rockfills on the surface of the dike slope. The p–y curves for rockfill can correspond to curves for sand with internal friction angles of 38 to 39 degrees [23]. Thus, the rockfill can be approximately regarded as sand with the aforementioned degrees. For wharf dikes with layered sandy soils, it is recommended that the equivalent angle of layered soils be taken as the weighted mean of the angles for various layers, which can be calculated by using the thickness of the layer as the weight. Then, the equivalent angle can be utilized for calculation of the depth to the point of fixity of the pile, which is expected to vary from approximately two times the pile diameter to approximately twelve times the pile diameter for wharf piles [4]. Therefore, the soil layers located twelve times the pile diameter below the dike surface can be ignored for the determination of the equivalent angle. Moreover, the impact of liquefaction for sandy soils was not incorporated in this study. Since the basic form of the formula for ductility capacity is established by using the equivalent cantilever concept to model the pile–soil interaction, the concept is not applicable where the soil response is significant. It is evident that the proposed formulas are not suitable for those situations.

7. Case Study

To verify the effectiveness and practicability of the proposed formulas in the actual engineering application, capacity analysis was conducted for an actual wharf with concrete

piles. The cross-sectional view of the wharf is shown in Figure 18. The superstructure consists of transverse cap beams with a width of 2.0 m and composite slabs with a thickness of 0.7 m. The spacing of the bent is 8.0 m. The width of the generally longitudinal beams is 1.6 m, while the crane beams have a width of 1.8 m. The piles have a diameter of 0.8 m and are made of C40 concrete. The individual pile is reinforced by 18 HRB400 bars with a diameter of 20 mm, resulting in a longitudinal reinforcement ratio ρ_l = 1.13%. The transverse reinforcement is provided by HPB 300 bars with a diameter of 16 mm at a pitch of 100 mm, resulting in a transverse reinforcement ratio ρ_s = 1.3%. A typical value of 40 kPa is utilized for the uniform live load. The properties of the dike soils are listed in Table 6.

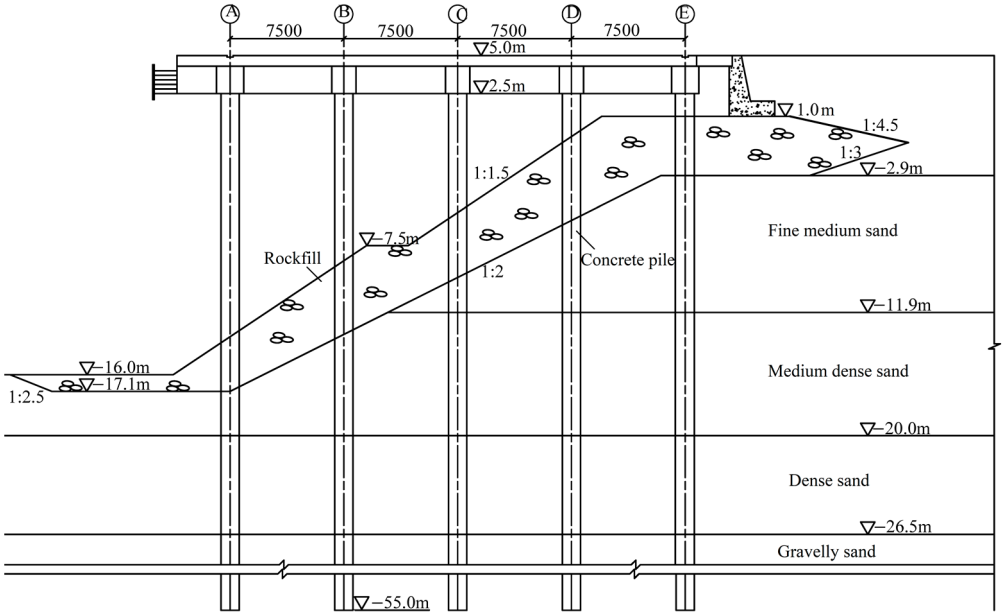


Figure 18. Cross-sectional view of the case study wharf (unit: mm).

Table 6. Soil properties for the case study wharf.

Soil Types	φ (°)	Effective Soil Weight (kN/m^3)
Rockfill	39.0	10.0
Fine medium sand	32.1	9.2
Medium dense sand	34.0	10.0
Dense Sand	36.0	10.5
Gravelly sand	38.2	11.1

Since the landward pile has the shortest length above ground level, the displacement capacity of the wharf is determined based on that pile. The axial load of the pile can be calculated from the gravity of the superstructure and live load, resulting in the axial load level $P_a/(f'_c A_g) = 0.129$. The axial load from the crane is ignored in the case study for ease. Considering the three performance levels in Table 2, the curvature ductility capacities for the pile sections can be determined by Equations (12)–(14), as listed in Table 7. According to the discussion in Section 6, an equivalent angle φ_E of layered soils is calculated as follows:

$$\varphi_E = \frac{39.0 \times 3.9 + 32.1 \times 5.7}{12 \times 0.8} = 34.9^\circ \quad (24)$$

in which the soil layers located twelve times the pile diameter below the dike surface were not included in the determination of the equivalent angle, and L_u/D was taken as 1.5/0.8 = 1.875. Then, the depth to the point of fixity L_f can be calculated from Equation (15), resulting in L_f = 5.427 m. Subsequently, the pile yield displacement can be computed by Equations (2), (11) and (16). Finally, the displacement ductility capacities of the pile for

Level I, Level II, and Level III are determined by Equations (18), (19) and (22), respectively, resulting in the displacement capacities listed in Table 7.

Table 7. Displacement capacities for the case study wharf.

Performance Level	μ_Φ	Δ_y (m) (Proposed Formulas)	Δ_y (m) (Pushover Analysis)	ψ	μ_Δ	Δ_c (m) (Proposed Formulas)	Δ_c (m) (Pushover Analysis)
Level I	3.901	0.0250	0.0209	0.423	2.227	0.0556	0.0506
Level II	5.538			0.962	5.366	0.1342	0.1193
Level II	16.591			0.454	8.078	0.2020	0.1750

To validate the applicability and accuracy of the proposed formulas, the two-dimensional numerical model of the entire wharf for pushover analysis was constructed based on the modeling method in Section 3.1. The *p*–*y* curves for sand with an internal angle of 39.0° were used to characterize the reaction of the rockfill. Then, nonlinear static pushover analysis was conducted to determine the displacement capacity for each performance level by monitoring the material strains in pile plastic regions, as listed in Table 7. The pushover curve of the entire wharf is graphically illustrated in Figure 19, in which the yield displacement and displacement capacities for all three levels are presented. It could be found that the ratios of displacement capacities calculated by the proposed formulas and those determined by pushover analysis were around 1.1, which validated the effectiveness and applicability of the proposed procedure. It seems that the formulas overestimated the displacement capacity of the wharf. However, the accuracy was generally adequate for a preliminary design.

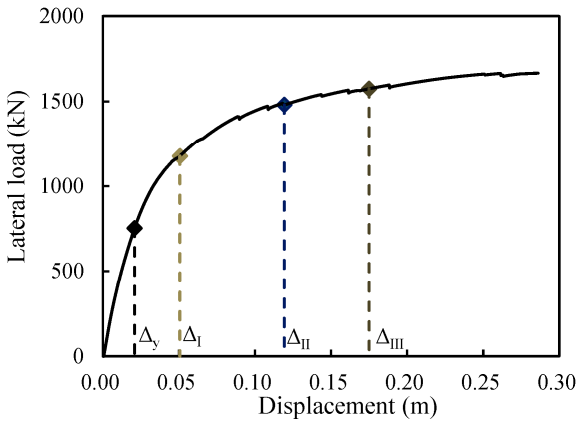


Figure 19. Pushover curve for entire wharf.

8. Conclusions

To supersede the displacement capacity analysis method with detailed pushover analysis in current seismic practices for wharves, a simplified procedure has been developed for concrete piles in wharves. The procedure can ensure that the material strain limits specified for the seismic performance level are not exceeded. The displacement capacity can be estimated by the product of the displacement ductility capacity and the yield displacement of piles. In order to obtain the closed-form formulas for ductility capacity and yield displacement, the equivalent cantilever concept is utilized to model the pile–soil interaction. Then, large quantities of nonlinear static pushover analyses for a fixed-head pile in homogeneous sand were conducted to determine the parameters in the formulas. Finally, a case study for an actual wharf was conducted to validate the effectiveness and applicability of the proposed formulas. Based on the results presented in the study, the primary conclusions are as follows:

1. The displacement ductility capacity for a specified performance level can be expressed as a function of the curvature ductility capacity of pile sections and parameter ψ. The curvature ductility capacity depends on the longitudinal and transverse steel ratio and the applied axial load from the superstructure of the wharf. The parameter ψ can be given by the function of the longitudinal and transverse steel ratio, unsupported length of the pile, and axial load level. The developed relationships are constructed based on concrete piles embedded in sand with specific reinforcing steel ratios, axial load levels, and dimensions, as listed in Tables 1 and 3. Thus, the proposed closed-form formulas can be applied to piles in sandy soils with longitudinal reinforcement ratios of 1~3%, transverse reinforcement ratios of 0.6~2%, unsupported lengths of $0D$~$6D$, and axial loads of $0.1f'_cA_g$~$0.3f'_cA_g$. For a pile with other conditions, the methodology in this study can be followed to develop similar relationships.
2. A transverse steel ratio with large values can increase the ductility capacity of piles. Thus, piles should be provided with adequate confining steel, especially at the pile–deck joint. However, a decrease in displacement ductility capacity with increasing longitudinal reinforcement ratio can be generally observed from the results of pushover analyses. Therefore, the volumetric ratio of longitudinal reinforcing steel should be limited to a reasonable range of 1% to 4%.
3. The axial load level will adversely influence the displacement ductility capacity of piles. It is recommended that the axial load level of concrete piles should be no more than 0.3, especially for landward piles. In order to reduce the applied load from the superstructure of the wharf, the rail girder should not directly locate upon the landward pile.

Author Contributions: Conceptualization, methodology, writing—review and editing, S.G.; formal analysis, Z.H.; formal analysis, Y.F. All authors have read and agreed to the published version of the manuscript.

Funding: This research was funded by the project ZR2024ME140 supported by Shandong Provincial Natural Science Foundation.

Data Availability Statement: All data, models, and code generated or used during the study appear in the submitted article.

Conflicts of Interest: The authors have no conflicts of interest to declare. All co-authors have seen and agreed with the contents of the manuscript. We certify that the submission is original work and is not under review at any other publication.

References

1. Chang, S.E. Disasters and transport systems: Loss, recovery and competition at the Port of Kobe after the 1995 earthquake. *J. Tran. Geog.* **2000**, *8*, 53–65. [CrossRef]
2. Werner, S.; McCullough, N.; Bruin, W.; Augustine, A.; Rix, G.; Crowder, B.; Tomblin, J. Seismic performance of Port de Port-au-Prince during the Haiti earthquake and post-earthquake restoration of cargo throughput. *Earthq. Spec.* **2011**, *27*, 387–410. [CrossRef]
3. Zhao, X.; Liao, X.; Hu, Z.; Li, X.; Nie, Y.; Liu, J.; Xu, Y. Seismic fragility analysis of steel pipe pile wharves with random pitting corrosion. *Buildings* **2023**, *13*, 2619. [CrossRef]
4. Port of Long Beach (POLB). *Wharf Design Criteria (Version 5.0)*; Port of Long Beach: California, CA, USA, 2021.
5. *ASCE/COPRI 61-14*; Seismic Design of Piers and Wharves. American Society of Civil Engineers: Reston, VA, USA, 2014.
6. Goel, R.K. Simplified procedure for seismic evaluation of piles with partial-moment connection to the deck in marine oil terminals. *J. Struct. Eng.* **2010**, *136*, 521–531. [CrossRef]
7. Zucca, M.; Franchi, A.; Crespi, P.; Longarini, N.; Ronca, P. The new foundation system for the transept reconstruction of the Basilica Di Collemaggio. In Proceedings of the 10th International Masonry Conference, Milan, Italy, 9–11 July 2018.
8. Budek, A.M.; Priestley, M.J.N.; Benzoni, G. Inelastic seismic response of bridge drilled-shaft RC pile/columns. *J. Struct. Eng.* **2000**, *126*, 510–517. [CrossRef]
9. Chai, Y.H. Flexural strength and ductility of extended pile-shafts. I: Analytical model. *J. Struc. Eng.* **2002**, *128*, 586–594. [CrossRef]
10. Chai, Y.H.; Hutchinson, T.C. Flexural strength and ductility of extended pile-shafts. II: Experimental study. *J. Struct. Eng.* **2002**, *128*, 595–602. [CrossRef]

11. Chai, Y.H.; Song, S.T. Assessment of seismic performance of extended pile-shafts. *Earth. Eng. Struct. Dyn.* **2003**, *32*, 1937–1954. [CrossRef]
12. Song, S.T.; Chai, Y.H.; Hale, T.H. Analytical model for ductility assessment of fixed-head concrete piles. *J. Struct. Eng.* **2005**, *131*, 1051–1059. [CrossRef]
13. Song, S.T.; Wang, C.Y.; Hu, T.F. Displacement ductility limits for pile foundations in cohesionless soils. *J. Earth. Eng.* **2018**, *22*, 595–629. [CrossRef]
14. Chiou, J.S.; Yang, H.H.; Chen, C.H. Plastic hinge setting for nonlinear pushover analysis of pile foundations. In Proceedings of the 14th World Conference of Earthquake Engineering, Beijing, China, 12–17 October 2008.
15. Chiou, J.S.; Tsai, Y.C.; Chen, C.H. Investigating influencing factors on the ductility capacity of a fixed-head reinforced concrete pile in homogeneous clay. *J. Mech.* **2012**, *28*, 489–498. [CrossRef]
16. *2A-WSD (RP 2A-WSD)*; Recommended Practice for Planning, Designing and Constructing Fixed Offshore Platforms-Working Stress Design. American Petroleum Institute: Washington, DC, USA, 2000.
17. Tuladhar, R.; Maki, T.; Mutsuyoshi, H. Cyclic behavior of laterally loaded concrete piles embedded into cohesive soil. *Earth. Eng. Struc. Dyn.* **2008**, *37*, 43–59. [CrossRef]
18. Mander, J.B.; Priestley, M.J.N.; Park, R. Theoretical stress-strain model for confined concrete. *J. Struct. Eng.* **1988**, *114*, 1804–1826. [CrossRef]
19. California Department of Transportation. *Seismic Design Specifications of Steel Bridges*; California Department of Transportation: Sacramento, CA, USA, 2016.
20. Abdelaziz, A.Y.; El Naggar, M.H.; Ouda, M. Determination of depth-of-fixity point for laterally loaded vertical offshore piles: A new approach. *Ocean Eng.* **2021**, *232*, 109113. [CrossRef]
21. *ACI-318*; Building Code Requirements for Structural Concrete and Commentary. American Concrete Institute: Farmington Hills, MI, USA, 2011.
22. New Zealand Transport Agency (NZTA). *Bridge Manual*; New Zealand Transport Agency: Willington, New Zealand, 2013.
23. Kawamata, Y. Seismic Performance of a Pile-Supported Container Wharf Structure in Rockfill. Ph.D. Thesis, Oregon State University, Portland, OR, USA, 2009.

Disclaimer/Publisher's Note: The statements, opinions and data contained in all publications are solely those of the individual author(s) and contributor(s) and not of MDPI and/or the editor(s). MDPI and/or the editor(s) disclaim responsibility for any injury to people or property resulting from any ideas, methods, instructions or products referred to in the content.